International Journal of Advance Research, IJOAR .org
Volume 4, Issue 5, May 2016, Online: ISSN 2320-9186

THEORETICAL ANALYSIS, FINITE ELEMENT METHOD AND OPTIMIZATION OF HEAT GENERATION IN FRICTION STIR WELDING FROM DIFFERENT PROBE AND SHOULDER PROFILES

Sabah Khammass Hussein

Abstract: --Based on the principle of the friction that produced from the contact surfaces between the tool and workpiece, the analytical models of heat generation from different probes and shoulders of friction stir welding tool have been derived. Five type of probe (cylindrical, quasi cone, square, hexagonal and multi-cylinder), shoulders (cylindrical, cylindrical - flat slot, cylindrical - double flat slot, cylindrical - single half circle slot and cylindrical - double half circle slot) and tools arms are used and considered as the levels of the Taguchi method. With the aid of Minitab program, this method proposed 25th type of tool design. The heat generation from each tool type has been calculated by finite element method using Comsol Multiphysics program. The effect of each type of probe, shoulder and tool arm on the change of heat generation has been analyzed. The design of experiment method is used to optimize the maximum heat generation from the proposed tool type. The maximum heat generated is observed in tool type which contains a hexagonal probe and circular slotted shoulder. Increase the number of slots in shoulder results in increase the generated heat. The tool arm which contains circumferential fins gives a higher heat as comparing with the smooth type.

Keywords: FSW, FEM, heat generation, Tool geometry, Welding, Friction welding, Stir welding.

1. INTRODUCTION:

DURING stir welding process, the temperature generated from the friction between the tool surfaces and workpiece is below the melting point, hence, a higher phase transformation is produced. The knowledge of temperature distribution through the welding regions takes a wide prospect. Due to the variation of temperature distribution through the weld metal, heat affected zone and the base metal; the mechanical and metallurgical properties will differ from region to another [1]. The evaluation of temperature and welding residual stress has been studied using FEM depending on the heat source generated from tool as well as to the convection and radiation of heat from the workpiece.

The thermo-mechanical process in FSW of aluminum alloy 6061 is studied using FEM based on the friction between the material and the tool. They presented the relation between the welding residual stress and welding parameters [2].

The analytical model of heat generated during welding process is established depending on the assumptions of the contact condition (sliding, sticking and partial sliding-sticking) between tool surfaces and the specimen. This model has been modified from the previous models. The proportional relationship between the applied force and the generated heat in the sliding condition is found [3].

A 3D FEM is used to predict the material flow and grain size during FSW with different tool geometries. The optimum advance speed and tool geometry is specified [4].

The transient thermal FE analysis is used to obtain the temperature distribution generated during FSW.

- Sabah Khammass Hussein: s currently pursuing Ph.D. degree in Mechanical *Engineering in Middle Technical University, Iraq. E*-mail: sabah.kh1974@yahoo.com

The source of heat generated from probe and tool is considered in the model building and gave a good simulation in predict the temperature distribution [5].

The strain change and thermo mechanical process are proposed in building the FEM of temperature distribution of FSW depending on Lagrangeian increment. The highest temperature is observed at the nugget zone with a V-shape temperature profile. The upper surface of workpiece gave a higher strain as compared with lower surface [6].

Comsol Multiphysics software is used to formulate the model of FEM in FSW. This model gave a good agreement with the measured experimental temperature data. The Taguchi method is used to optimize the maximum temperature according to the input parameters [7].

ANSYS program is used to simulate and develop the model of FEM in FSW. A good agreement is found between the proposed FE model and the experimental data [8].

The effect of different tool geometries on the strength and microstructure of FSW has been studied. It was observed that the strength and micro-hardness of weldment change with changing the tool geometry [9].

Three different tool pin shape (straight cylindrical threaded and square) is used in FSW of Aluminum alloy. It observed that the threaded pin profile type give a good mechanical properties as compared with the other [10].

2. HEAT GENERATION IN SHOULDER AND PROBE:

The generated heat during FSW depends on the contact shear stress between tool and workpiece [3]. The following model is assumed to evaluate the generated heat in shoulder and probe:

$$dQ = \omega dM = \omega . r . dF = \omega . r . \tau . dA \quad (1)$$

$$Q = \omega . \tau \int r . dA \quad (2)$$

Where:

Q: heat generation in shoulder or probe (W), ω: angular velocity of tool (Rad.sec^{-1}.), r: cylindrical coordinate (m), M: moment (N.m), F: shear force (N), A: contact area (m^2), τ : shear stress (Mpa),

According to Eq. (2), the heat in the simplest cylindrical shoulder type, figure (1) is:

$$Q = \omega . \tau \int_0^{2\pi} \int_{Rp}^{Rs} r^2 . dr d\theta = \frac{2\pi\omega\tau}{3}(Rs^3 - Rp^3) \quad (3)$$

$$A = \pi(Rs^2 - Rp^2) \quad (4)$$

The generated heat per unit area is, q (W.m^{-2}):

$$q = \frac{Q}{A} \quad (5)$$

$$\therefore q = \frac{2\omega\tau}{3}\frac{(Rs^3 - Rp^3)}{(Rs^2 - Rp^2)} \quad (6)$$

On the other hand, for the cylindrical probe, the heat is generated from the tip and side surface (Q1 and Q2 respectively), figure (2). Thus:

$$Q_1 = \omega . \tau \int_0^{2\pi} \int_0^{r} r^2 . dr d\theta = \frac{2\pi\omega\tau}{3} r^3 \quad (7)$$

$$A_1 = \pi r^2, \quad \text{according to Equation (5)} \rightarrow q_1 = \frac{2\omega\tau}{3} r \quad (8)$$

And for the side surface;

$$Q_2 = \omega . \tau \int_0^{h} \int_0^{2\pi} r^2 . d\theta dz = 2\pi\omega\tau r^2 h \quad (9)$$

$$A_2 = 2\pi r h, \quad \text{according to Equation (5)} \rightarrow q_2 = \omega\tau r \quad (10)$$

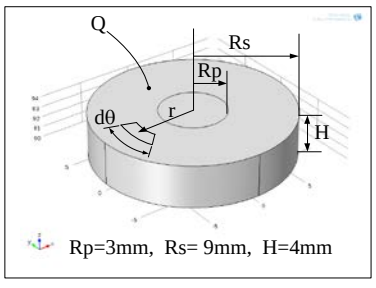

Fig. 1 cylindrical shoulder

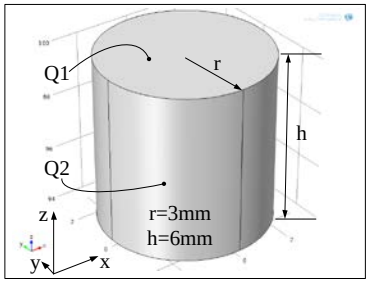

Fig. 2 cylindrical probe

Based on this model [3], eq. (2), the heat generates from the other four types of shoulder and probe is derived as following:

2.1 Heat generation model in the proposed shoulder types

2.1.1 Cylindrical shoulder with flat slot:

It assumed that the shoulder surface is inserting through the workpiece during the welding process with a height (h), figure (3 and 4). According to this assumption, five surfaces will generate heat for single slot, figure (3);

$$Q_1 = \omega.\tau \int_0^h \int_0^{2\pi} Rp^2 \,.\, d\theta dz = 2\pi\omega\tau Rp^2 h \qquad 11)$$

$$Q_2 = \omega.\tau \int_0^{2\pi} \int_{Rp}^{R_1} r^2 \,.\, dr d\theta = \frac{2\pi\omega\tau}{3}\left({R_1}^3 - Rp^3\right) \qquad (12)$$

$$Q_3 = \omega.\tau \int_0^h \int_0^{2\pi} {R_1}^2 \,.\, d\theta dz = 2\pi\omega\tau {R_1}^2 h \qquad (13)$$

$$Q_4 = \omega.\tau \int_0^{2\pi} \int_{R_1}^{Rs} r^2 \,.\, dr d\theta = \frac{2\pi\omega\tau}{3}\left(Rs^3 - {R_1}^3\right) \qquad (14)$$

$$Q_5 = \omega.\tau \int_0^h \int_0^{2\pi} {R_s}^2 \,.\, d\theta dz = 2\pi\omega\tau {R_s}^2 h \qquad (15)$$

The area and the generated heat per unit area (q) from each section are given as follow:

$$A_1 = 2\pi Rph,\ \ q_1 = \omega\tau Rp \qquad (16)$$

$$A_2 = \pi\left({R_1}^2 - Rp^2\right),\quad q_2 = \frac{2\omega\tau}{3}\frac{\left({R_1}^3 - Rp^3\right)}{\left({R_1}^2 - Rp^2\right)} \qquad (17)$$

$$A_3 = 2\pi R_1 h,\ \ q_3 = \omega\tau R_1 \qquad (18)$$

$$A_4 = \pi\left(Rs^2 - {R_1}^2\right),\quad q_4 = \frac{2\omega\tau}{3}\frac{\left(Rs^3 - {R_1}^3\right)}{\left(Rs^2 - {R_1}^2\right)} \qquad (19)$$

$$A_5 = 2\pi R_s h,\quad q_3 = \omega\tau R_s \qquad (20)$$

For double slot shoulder surface, figure (4), the nine heat generations are derived with the same previous procedure, table (1);

TABLE 1
HEAT GENERATION FROM DOUBLE SLOT SHOULDER

No.	Q	$Eq.$	A	q	$Eq.$
1	$2\pi\omega\tau Rp^2 h$	21	$2\pi R_p h$	$\omega\tau R_p$	30
2	$\frac{2\pi\omega\tau}{3}\left({R_1}^3 - Rp^3\right)$	22	$\pi\left({R_1}^2 - {R_p}^2\right)$	$\frac{2\omega\tau}{3}\frac{\left({R_1}^3 - {R_p}^3\right)}{\left({R_1}^2 - {R_p}^2\right)}$	31
3	$2\pi\omega\tau {R_1}^2 h$	23	$2\pi R_1 h$	$\omega\tau R_1$	32
4	$\frac{2\pi\omega\tau}{3}\left({R_2}^3 - {R_1}^3\right)$	24	$\pi\left({R_2}^2 - {R_1}^2\right)$	$\frac{2\omega\tau}{3}\frac{\left({R_2}^3 - {R_1}^3\right)}{\left({R_2}^2 - {R_1}^2\right)}$	33
5	$2\pi\omega\tau {R_2}^2 h$	25	$2\pi R_2 h$	$\omega\tau R_2$	34
6	$\frac{2\pi\omega\tau}{3}\left({R_3}^3 - {R_2}^3\right)$	26	$\pi\left({R_3}^2 - {R_2}^2\right)$	$\frac{2\omega\tau}{3}\frac{\left({R_3}^3 - {R_2}^3\right)}{\left({R_3}^2 - {R_2}^2\right)}$	35
7	$2\pi\omega\tau {R_3}^2 h$	27	$2\pi R_3 h$	$\omega\tau R_3$	36
8	$\frac{2\pi\omega\tau}{3}\left(Rs^3 - {R_3}^3\right)$	28	$\pi\left({R_s}^2 - {R_3}^2\right)$	$\frac{2\omega\tau}{3}\frac{\left({R_s}^3 - {R_3}^3\right)}{\left({R_s}^2 - {R_3}^2\right)}$	37
9	$2\pi\omega\tau Rs^2 h$	29	$2\pi R_s h$	$\omega\tau R_s$	38

Or, in general form, the heat generated per unit area in this type of shoulder is:

$$q = \omega\tau\left(\sum R_i + \frac{2}{3}\sum \frac{\left({R_{outer)i}}^3 - {R_{inner)i}}^3\right)}{\left({R_{outer)i}}^2 - {R_{inner)i}}^2\right)}\right) \qquad (39)$$

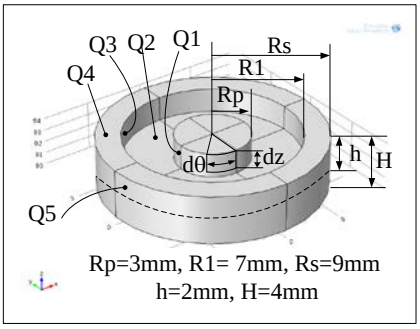

Fig. 3 Cylindrical shoulder with single flat slot

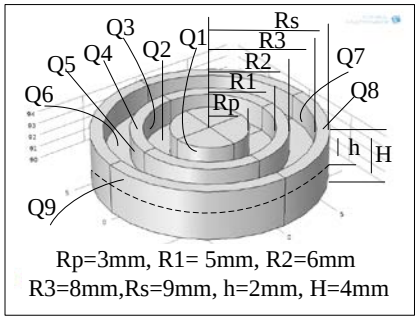

Fig. 4 Cylindrical shoulder with double flat slot

2.1.2 Cylindrical shoulder with half circle slot:

For a single slot, figures (5), there are a three type of heat that can be generate from surface.
The first and last heat (Q1 and Q3) generate with the inserted height (h). In order to drive the first heat generated (Q1), a half section is assumed, figure (6). According to Eq. (2), this heat will be;

$$Q_1 = \omega.\tau \int x\,.\,dA = 2\pi\omega\tau \int x\,.\,x\sqrt{1 + \left(\frac{dx}{dy}\right)^2}\ dy =$$
$$2\pi\omega\tau R\left[R^2\left(\frac{\theta}{2} + \frac{\sin 2\theta}{4}\right) + 2xoR\sin\theta + xo^2\theta\right]_{\theta 1}^{\theta 2} \qquad (40)$$

Where:

$x = xo + \sqrt{R^2 - (y - yo)^2}\,, \theta_1 = \tan^{-1}(H/Rp)$ and $\theta_2 = \tan^{-1}((H/(Rp + 2R))$

The second surface heat generation is:

$$Q_2 = \omega.\tau \int_0^{2\pi} \int_{R_s}^{Rp+2R} r^2\,.\,dr d\theta = \frac{2\pi\omega\tau}{3}\left({R_s}^3 - (R_p + 2R)^3\right) \quad (41)$$

$$Q_3 = \omega.\tau \int_0^{R} \int_0^{2\pi} {R_s}^2\,.\,d\theta dz = 2\pi\omega\tau {R_s}^2 R \quad (42)$$

The area and generated heat per unit area for each region will be:

$$A_1 = 2\pi \int x.\sqrt{1 + \left(\frac{dx}{dy}\right)^2}\ dy = 2\pi R[R\sin\theta + xo.\theta]_{\theta 1}^{\theta 2},\ q_1 = \frac{2\pi\omega\tau R\left[R^2\left(\frac{\theta}{2} + \frac{\sin 2\theta}{4}\right) + 2xoR\sin\theta + xo^2\theta\right]_{\theta 1}^{\theta 2}}{2\pi R[R\sin\theta + xo.\theta]_{\theta 1}^{\theta 2}} \quad (43)$$

$$A_2 = \pi\left({R_s}^2 - (R_p + 2R)^2\right), \quad \rightarrow q_2 = \frac{2\omega\tau}{3}\frac{\left({R_s}^3 - (R_p + 2R)^3\right)}{\left({R_s}^2 - (R_p + 2R)^2\right)} \quad (44)$$

$$A_3 = 2\pi R_s R, \quad \rightarrow q_3 = \omega\tau R_s \quad (45)$$

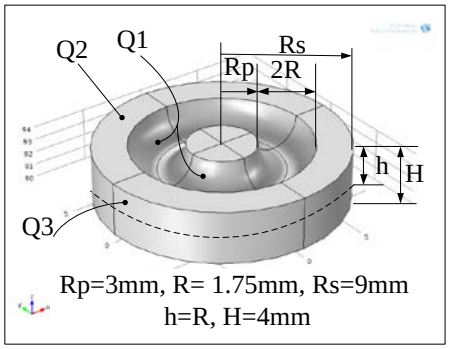

Fig. 5 Cylindrical shoulder with single half circle slot

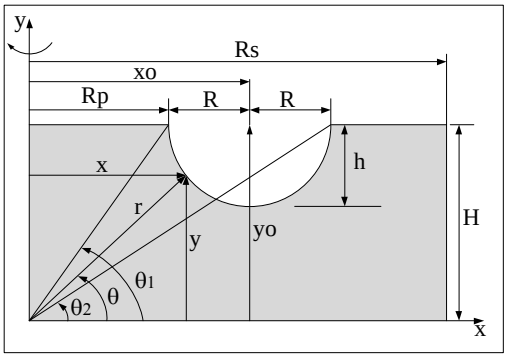

Fig. 6 Half section of shoulder

In the same manner, the generated heat for double slot, figure (7) will be:
From figure (8),

$$Q_1 = 2\pi\omega\tau R\left[R^2\left(\frac{\theta}{2} + \frac{\sin 2\theta}{4}\right) + 2xo_1 R\sin\theta + {xo_1}^2\theta\right]_{\theta 1}^{\theta 2} \quad (46)$$

Where:

$xo_1 = Rp + R, \quad \theta_1 = \tan^{-1}(H/Rp)$ and $\theta_2 = \tan^{-1}\left((H/(Rp + 2R)\right)$ (47)

$$Q_2 = \omega.\tau \int_0^{2\pi} \int_{R_1}^{Rp+2R} r^2\,.\,dr d\theta = \frac{2\pi\omega\tau}{3}\left({R_1}^3 - \left(R_p + 2R\right)^3\right) \quad (48)$$

$$Q_3 = 2\pi\omega\tau R\left[R^2\left(\frac{\theta}{2} + \frac{\sin 2\theta}{4}\right) + 2xo_2 R\sin\theta + {xo_2}^2\theta\right]_{\theta 3}^{\theta 4} \quad (49)$$

Where:

$xo_2 = R_1 + R, \ \theta_3 = \tan^{-1}(H/R_1)$ and $\theta_4 = \tan^{-1}((H/(R_1 + 2R))$

$$Q_4 = \omega.\tau \int_0^{2\pi} \int_{R_s}^{R_1+2R} r^2\,.\,dr d\theta = \frac{2\pi\omega\tau}{3}\left({R_s}^3 - (R_1 + 2R)^3\right) \quad (50)$$

$$Q_5 = \omega.\tau \int_0^{R} \int_0^{2\pi} {R_s}^2\,.\,d\theta dz = 2\pi\omega\tau {R_s}^2 R \quad (51)$$

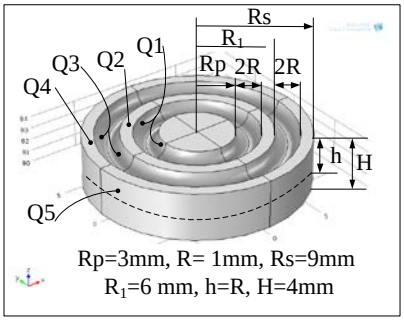

Fig. 7 Cylindrical shoulder with double half circle slot

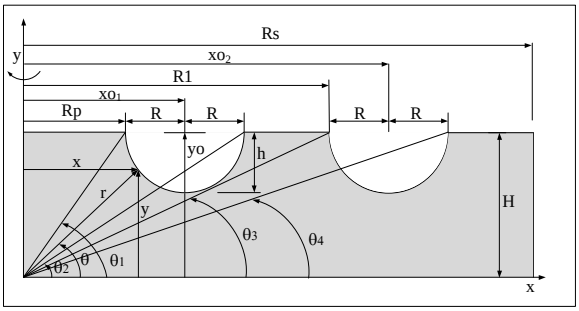

Fig. 8 Half section of shoulder

2.2 Heat generation model in the proposed probe types

2.2.1 Quasi cone probe:

This type of probe generates the heat from two surfaces, the surrounding and tip surfaces (Q1 and Q3 respectively), figure (9). The first heat (Q1) can be evaluated with the aid of figure (10) as follow:

$$Q_1 = \omega.\tau \int x\,.\,dA = 2\pi\omega\tau \int x.x\sqrt{1 + \left(\frac{dx}{dy}\right)^2}\ dy = \frac{2\pi\omega\tau}{3}\sqrt{h^2 + (r_2 - r_1)^2}\,(r_1^2 + r_1 r_2 + r_2^2) \quad (52)$$

Where:

$$x = r_1 + \frac{r_2 - r_1}{h} y$$

According to Eq. (2), the second heat will be:

$$Q_2 = \frac{2\pi\omega\tau}{3} {r_2}^3 \quad (53)$$

The magnitude of area and q will be as follow:

$$A_1 = 2\pi \int x . \sqrt{1 + \left(\frac{dx}{dy}\right)^2}\ dy =$$
$$\pi(r_1 + r_2)\sqrt{h^2 + (r_2 - r_1)^2},\ q_1 = \frac{2\omega\tau}{3} \frac{({r_1}^2 + r_1 r_2 + {r_2}^2)}{(r_1 + r_2)} \quad (54)$$

$$A_2 = \pi {r_2}^2,\ \rightarrow q_2 = \frac{2\omega\tau}{3} r_2 \quad (55)$$

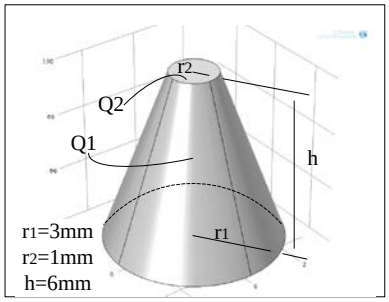

Fig. 9 Quasi cone probe

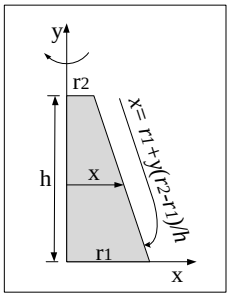

Fig. 10 Half section of quasi cone probe

2.2.2 Square probe:
There are two regions that generate heat from probe, side region (from each square face) and the square tip of probe, figure (10 and 11). In order to derive the heat of each region, the following steps are considered:

$$Q_1 = 8.\omega.\tau \int_0^h \int_0^a a\,.\,dydz = 8\omega\tau a^2 h \quad (56)$$

$$A_1 = 8ah,\ \rightarrow q_1 = \omega\tau a \quad (57)$$

$$Q_2 = 8\omega.\tau \int_0^{\pi/4} \int_{r_1}^{r_2} r^2\,.\,drd\theta = \frac{2\pi\omega\tau a^3}{3}\left(2\sqrt{2} - 1\right) \quad (58)$$

$$A_2 = 4a^2,\ \rightarrow q_2 = \frac{\pi\omega\tau a}{6}\left(2\sqrt{2} - 1\right) \quad (59)$$

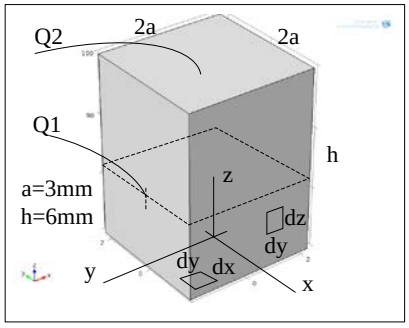

Fig. 11 Square probe

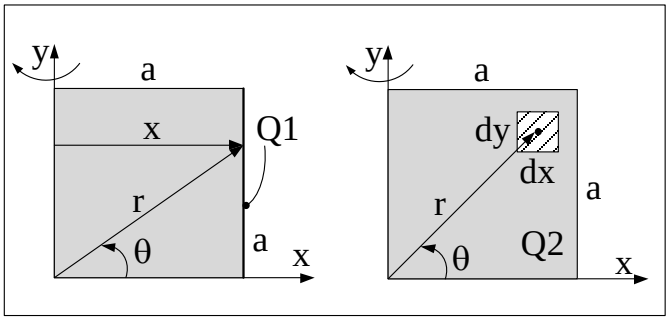

Fig. 12 Side and tip section

2.2.3 Hexagonal probe:
As presented in figure (13 and 14), and according to the dimensions mentioned in those figure, the two the equations of heat generated from the side and tip of probe are as follow:

$$Q_1 = 12.\omega.\tau \int_0^h \int_0^b a\,.\,dydz = 12\omega\tau a^2 h \quad (60)$$

$$A_1 = 12ah,\quad q_1 = \omega\tau a = \omega\tau r_p.\cos 30 \quad (61)$$

$$Q_2 = 12\omega.\tau \int_0^{\theta_1} \int_a^{r_p} r^2\,.\,drd\theta = \frac{2\pi(1 - \cos 30^3)}{3} \omega\tau {r_p}^3 \quad (62)$$

Where: $\theta_i = \omega/6$

$$A_2 = 3\sin 60.{r_p}^2,\ q_2 = \frac{2\pi(1 - \cos 30^3)}{9.\sin 60}\omega\tau r_p$$

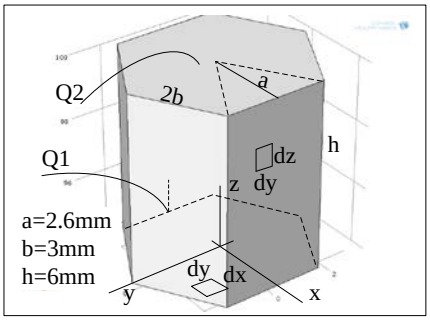

Fig. 13 Hexagonal probe

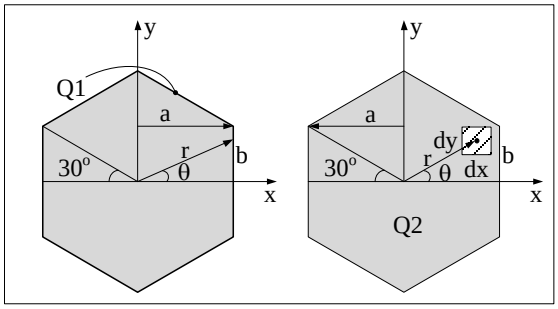

Fig. 14 Side and tip section

2.2.4 Multi-cylinder probe:
In this type, figure (15), the heat generated will be the summation of heat for each cylindrical probe as in figure (2):

$$Q_{side} = 2\pi\omega\tau \sum_{i=0}^{5} r_i^2 t_i \quad (64)$$

$$A_1 = 2\pi \sum_{i=0}^{5} r_i t_i, \; q_1 = \omega\tau \sum_{i=0}^{5} r_i \quad (65)$$

$$Q_{tip} = \frac{2\pi\omega\tau}{3} \sum_{i=0}^{5} (r_{outer})_i^3 - (r_{inner})_i^3 \quad (66)$$

$$A_2 = \pi \sum_{i=0}^{5} (r_{outer})_i^2 - (r_{inner})_i^2 \quad (67)$$

according to Equation (5)

$$q_2 = \frac{2\omega\tau}{3} \sum_{i=0}^{5} \frac{(r_{outer})_i^3 - (r_{inner})_i^3}{(r_{outer})_i^2 - (r_{inner})_i^2} \quad (68)$$

3. Convection and radiation heat from tool arm:

It considered that the heat transfer between tool arm side surface and surrounding include both convection and radiation [11];

$$-k\frac{\partial T}{\partial x} = \sigma\varepsilon\left(T^4 - T_a^4\right) + h(T - T_a) \quad (69)$$

Where:

σ: Stefan − Boltzmann constant (5.67 $* 10^{-8}$ W.m^{-2}.K^{-4})
ε: emissivity (0.75)
Ta: ambient temperature (300 K)
h: heat transfer coefficient (15 W/m2.K)

A five type of tool arm are used in this work, figure (16). The nominal diameter and height are (18 and 90 mm respectively).

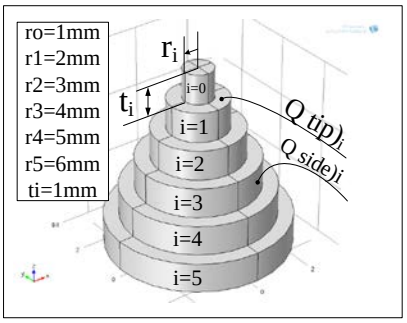

Fig. 15 Multi-cylinder probe

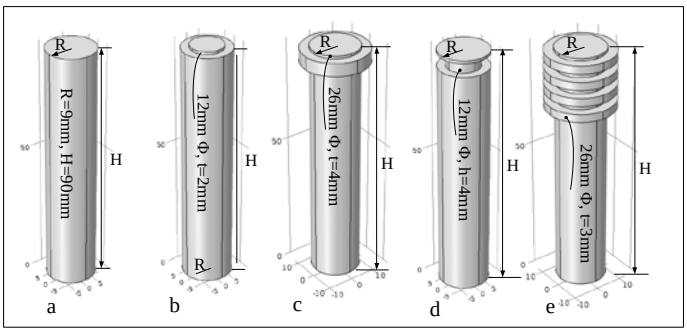

Fig. 16 Tool arm types

4. Tool Design models by Taguchi method:

The optimization of heat generation from tool can be developed by change the shape of probe, shoulder and tool arm. Five types for each of probe, shoulder and tool arm are used as mention in figures (1-14).
Each of those parts can be assembled with a complete design tool model (tool arm+ shoulder +probe) by Taguchi method. The following codes are used in this method, table (2);
As a result from the above table, the number of factors is three (tool arm, shoulder and probe) and five levels for each factor. A Taguchi L25 orthogonal array is suggested from the Minitab program, table (3).
According to tool number in table (3), the shape of each tool design is shown in figure (17).

TABLE 2
CODES OF TOOL PARTS

Tool arm		Shoulder		pin	
type	Code	Type	Code	Type	Code
a	1	cylindrical	1	cylindrical	1
b	2	cylindrical - flat slot	2	quasi cone	2
c	3	cylindrical - double flat slot	3	square	3
d	4	cylindrical - single half circle slot	4	hexagonal	4
e	5	cylindrical - double half circle slot	5	multi-cylinder	5

TABLE 3
TOOL DESIGN BY TAGUCHI METHOD L25

Tool Arm	1	1	1	1	1	2	2	2	2	2	3	3	3	3	3	4	4	4	4	4	5	5	5	5	5
Shoulder	1	2	3	4	5	1	2	3	4	5	1	2	3	4	5	1	2	3	4	5	1	2	3	4	5
pin	1	2	3	4	5	2	3	4	5	1	3	4	5	1	2	4	5	1	2	3	5	1	2	3	4
Tool No.	1	2	3	4	5	6	7	8	9	10	11	12	13	14	15	16	17	18	19	20	21	22	23	24	25

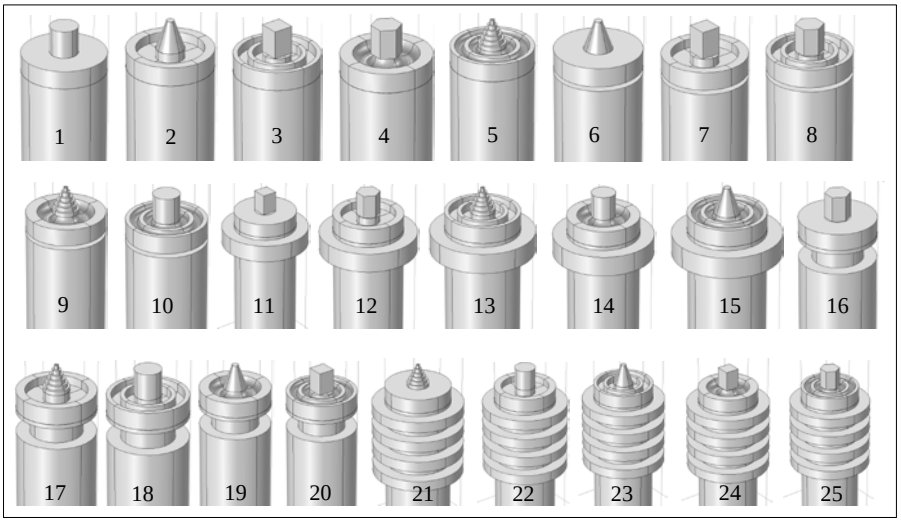

Fig. 17 The proposed tool design from Taguchi method

5. FINITE ELEMENT MODEL OF FSW TOOLS:

A Comsol Multiphysics program is used to formulate the finite element model for the previous 25th tool geometries. The analysis of heat transfer depends on the 1st law of thermodynamics. The temperature values and distribution in each tool is evaluated by solving the following differential equation;

$$\nabla.(k.\nabla T) + Q = \rho C_p\, u.\nabla T \qquad (70)$$

Where:
k: thermal conductivity (W/m K)
Q: heat generated from shoulder and probe (W)
ρ: density (kg/m^3)
Cp : specific heat capacity (kJ/kg.K)
u : velocity vector (m/s)
In order to build the finite element model, it assumed the type welded specimen material is (AA 6061) of (3mm thickness). The melting point is (900K). The welding parameters are (welding speed = 15 mm/min, rotating speed = 500 RPM).
The boundary conditions are applied according to the equations of heat source for each type of probe and shoulder of tool model as well as to the convection and radiation heat that occurs from the tool arm. An example of boundary conditions is presented in figure (18) for first tool model. A fine mesh is used for each model, figure (19) tool model 23.

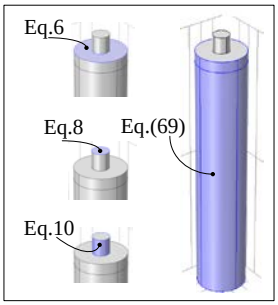

Fig. 18 boundary conditions for tool model-1

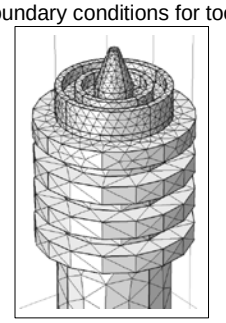

Fig. (19 Mesh of tool model -23

6. EXPERIMENTAL WORK:

In order to validate the derived analytical model, the temperature is recorded by means of (IR-device) along the tool surface during the welding process, figure (20). The proposed tool from Taguchi method (No.2) is manufactured from (O1 tool steel type-ASTM A681 [12]). The geometry of this tool is shown in figure (21). A good agreement is found (Texp. = 375 K, TFEM= 395 K).

Fig. 20 Temperature record during FSW process

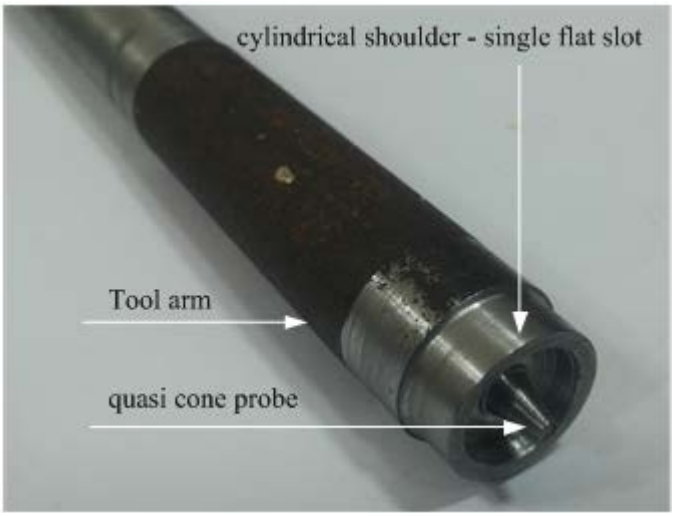

Fig. 21 Tool design (No. 2)

7. RESULTS AND DISCUSSIONS:

The tool models present in figure (17) has been tested according to the same input data mentioned in section (5) and its dimensions figures (1-16). It's required to maximize the heat generated from each model. The results of heat generated for each tool from the model of FE are presented in figure (22). As it has been observed, the minimum and maximum heat is found in tools (1 and 25 respectively).

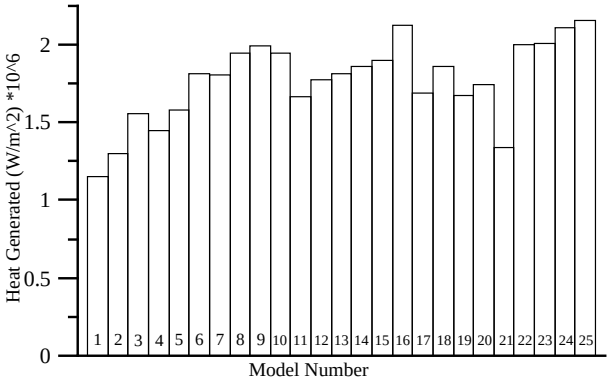

Fig. 22 Heat generated of tools from FEM

In order to recognize the effect of each type of probe, shoulder and tool arm on the generated heat, the results of mean effect and signal-to-noise graph in Taguchi method is shown in figures (23 and 24 respectively). From Taguchi analysis, it can be concluded that the heat generated has the maximum value in tool-25. This tool model includes the tool arm-5, shoulder-5 and probe-4.

The cylindrical shape of tool arm-1 gave least heat, while, increasing the number of fins increase the heat generation during the FSW processing as in tool arm-5. Increasing the number of slot in shoulder results in increasing the heat generated for each type of flat and circular slot. This reason can be consoled to the fact; increasing the frictional surface area results in increasing the generated heat.

Approximately, the same heat generated is observed in the cylindrical, quasi cone and square type of probe. But the highest surface area type (hexagonal probe type) gave the highest heat generated. The dispersion heat is observed in multi-cylinder probe.

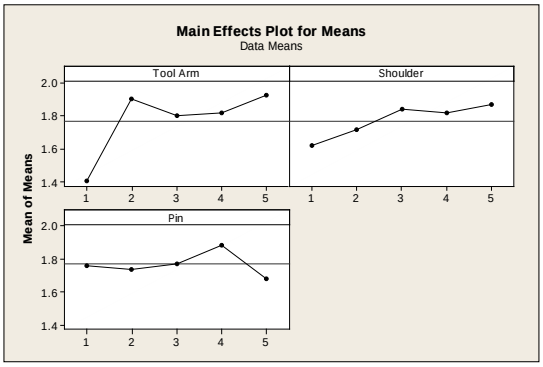

Fig. 23 Main effect plot

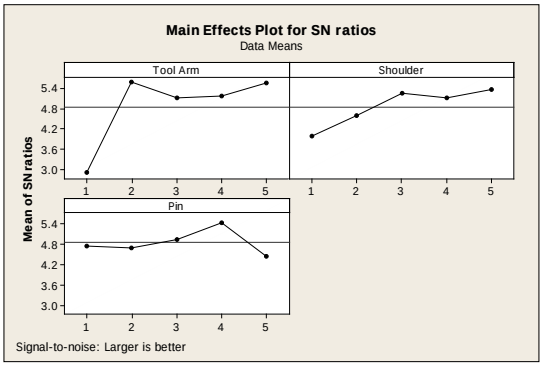

Fig. 24 Signal -to- noise graph

The tool parts that maximize and minimize the heat values can be summarized in table (3)

TABLE 4
TOOL PART NUMBERS WHICH MAXIMIZE AND MINIMIZE HEAT

	Tool arm	shoulder	probe
Maximize	5	5	4
Minimize	1	1	5

Tool-21 is selected as an example of temperature distribution resulted from FE mode. As it observed from figure (25), the higher ranges of temperature distribution concentrate in the region of probe and shoulder. This ranges decrease gradually through the longitudinal axis away from the probe tip.
At the contact region between the shoulder surface and workpiece, the higher ranges of temperature distribution is observed with an approximate constant values of temperature through the radius of shoulder, figure (26).

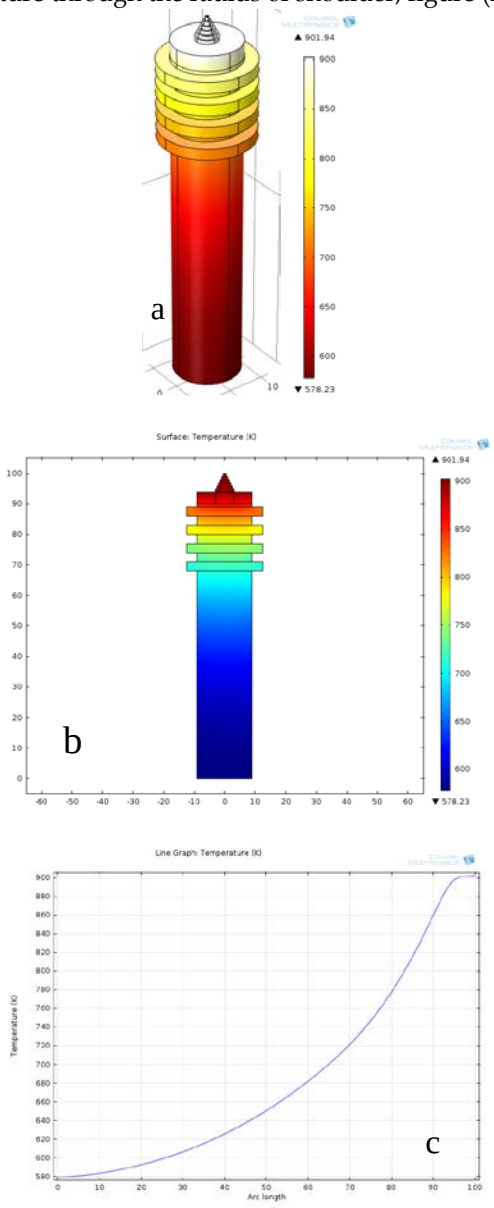

Fig. 25 Temperature distribution in tool-21 (a) 3D distribution (b) cross section (c) through the longitudinal axis

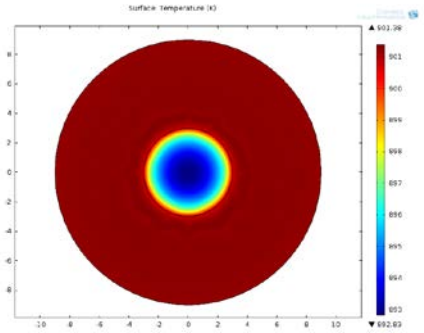

Fig. 26 Temperature distribution in shoulder-1 of tool-21

8. CONCLUSIONS:

1- A smooth cylindrical tool arm gave a minimum heat as comparing with those of fins.
2- Increasing the number of fins in tool arm increase the generated heat.
3- Flat cylindrical shoulder gave the minimum heat as comparing with the slotted shoulder.
4- The circular slotted shoulder produces a higher heat as comparing with the flat slot.
5- Increasing the number of slot in shoulder results in increasing the generated heat.
6- The minimum and maximum generated heat is found in multi-cylindrical and hexagonal probe respectively.
7- A hexagonal probe with the presents of fins in tool arm and the circular slots in shoulder gave the maximum generated heat in tool model during FSW.
8- A smooth type of tool arm and shoulder with multi-cylindrical probe gave the minimum generated heat in tool model during FSW.

REFERENCES:

[1] Rajiv S. Mishra and Murray W. Mahoney, "Friction Stir Welding and Processing", *ASM International, 2007.*

[2] C.M. Chen and R. Kovacevic, "Finite element modeling of friction stir welding-thermal and thermo-mechanical analysis", *International Journal of Machine Tools & Manufacture, V.43, 2003.*

[3] H Schmidt, J Hattel and J Wert "An analytical model for the heat generation in friction stir welding", *Modelling Simul. Mater. Sci. Eng. V.12, pp. 143-157, 2004.*

[4] G. Buffa, J. Huaa, R. Shivpuri and L. Fratini " Design of the friction stir welding tool using the continuum based FEM model", *Materials Science and Engineering A 419,pp.381-388,2006.*

[5] Binnur Goren Kiral1, Mustafa Tabanoglu and H. Tarik Serindag, " finite elewment modeling of friction stir welding in aluminum alloys joint", *Mathematical and Computational Applications, V.18, No.2, pp.122-131, 2013*

[6] Rahul Jain, S.K. Pal and S.B. Singh "Finite Element Simulation of Temperature and Strain Distribution in Al2024 Aluminum Alloy by Friction Stir Welding", *5th International & 26th All India Manufacturing Technology, Design and Research Conference (AIMTDR 2014) December 12th–14th, 2014.*

[7] Renju Mohan, N. R. Rajesh and Satheesh Kumar " finite element modeling for maximum temperature in friction stir welding of AA1100 and optimization of process parameters by Taguchi method " *International Journal of Research in Engineering and Technology, V. 03 Issue: 05 | May-2014.*

[8] Amay Deorao Meshram " Finite Element Modeling of Friction Stir Welding-Thermal Analysis", *International Journal of Engineering Research & Technology, V. 3 Issue 1, January -2014.*

[9] H. K. Mohanty, M. M. Mahapatra, P. Kumar, P. Biswas, and N. R. Mandal, " Effect of Tool Shoulder and Pin Probe Profiles on Friction Stirred Aluminum Welds - a Comparative Study", *J. Marine Sci. Appl. V.11, pp. 200-207, 2012.*

[10] Ram Niwas Bishnoia, Pawan Kumar Saprab and Raman Bhambhuc " Effect of Tool Pin Profile on Mechanical Properties of Single and Double Sided Friction Stir Welded Aluminum Alloy AA19000", *International Journal of Current Engineering and Technology, V.3, No.4, October 2013.*

[11] J. P. Holman, "*Heat Transfer*", McGraw-Hill Companies, Inc., 2010

[12] American Society for Test ing and Materials (ASTM), "*Standard Specification for Tool Steels Alloy*", ASTM A681 – 94, 1999.